Key Points:
- Dynamical variability can completely mask the BDC trend for periods shorter than around 12 years
- Time of Emergence of modeled BDC increase is calculated to be around 30 years consistent with observations
- This exceeds the length of some observational analyses

The influence of dynamical variability on the observed Brewer-Dobson circulation trend

Steven C. Hardiman[1] [iD], **Pu Lin[2]** [iD], **Adam A. Scaife[1]** [iD], **Nick J. Dunstone[1]** [iD], and **Hong-Li Ren[3]** [iD]

[1]Met Office, Exeter, UK, [2]Princeton University and NOAA/Geophysical Fluid Dynamics Laboratory, Princeton, New Jersey, USA, [3]Laboratory for Climate Studies, National Climate Center, China Meteorological Administration, Beijing, China

Abstract The strength of the Brewer-Dobson circulation (BDC) is predicted to increase due to climate change. However, this increase has yet to be robustly detected in observational analyses. In this study a long control simulation is used to calculate the Time of Emergence of the BDC trend and how much of that trend may be masked by dynamical variability in current observations. A Time of Emergence of around 30 years is found (assuming a 2%/decade trend in the BDC), similar to the length of current reanalysis data sets. However, the discrepancies in vertical velocities between different reanalysis products remain far larger than any predicted trend. Furthermore, dynamical variability can completely mask the BDC trend on time scales shorter than around 12 years. Thus, more robust observational analyses of vertical velocity are likely to be needed for at least the next decade before detection of a statistically significant trend can be expected.

1. Introduction

The Brewer-Dobson circulation (BDC) [*Butchart*, 2014] describes the stratospheric meridional mass circulation encompassing the upwelling of air from troposphere to stratosphere in the tropics, the poleward transport of air throughout the stratosphere, and the descent of this air back into the troposphere in the middle and high latitudes. The vertical structure of the BDC, consisting of shallow and deep circulations [*Birner and Boenisch*, 2011], is complicated, as is the way this structure is projected to evolve in response to climate change [*Lin and Fu*, 2013; *Hardiman et al.*, 2014]. In the present study, the commonly used definition of the vertical mass flux across 70 hPa is used to define the strength of the BDC. However, we use a mean over December–January–February (DJF) rather than the more usual annual mean, as explained further in section 2. At 70 hPa, an increase of 2%/decade in the strength of the BDC is expected due to climate change, as predicted by model simulations [*Butchart and Scaife*, 2001; *Butchart et al.*, 2006]. In practice, there is significant uncertainty in this 2%/decade value. For example, *Butchart et al.* [2010] find that the standard error for the DJF mean trend covers the range 1.3–2.2%/decade for the moderate Special Report on Emissions Scenarios (SRES) A1B scenario [*Nakicenovic and Swart*, 2000], and *Butchart* [2014] find that the standard error in the annual mean trend covers the range 2.5–3.9%/decade for the more extreme Representative Concentration Pathway (RCP) 8.5 scenario [*Riahi et al.*, 2007; *Moss et al.*, 2010]. In the present study, we primarily use the value 2%/decade in order to draw some qualitative conclusions and just use the above range (1.3–3.9%/decade) to provide an estimate of uncertainty.

Using observations of lower stratospheric temperatures, *Fu et al.* [2015] claim that a strengthening of the BDC, consistent with this 2%/decade prediction, is now detectable. However, this study depends on being able to isolate the "dynamic component" of the lower stratospheric temperature changes associated with the BDC. Measurements more widely used to infer the strength of the BDC have yet to detect an increasing trend in the BDC. For example, using stratospheric age of air [*Waugh*, 2009] to infer the strength of the stratospheric circulation, *Engel et al.* [2009] report no trend (though note that age of air is not directly comparable with the vertical mass flux used to define the BDC) [*Garny et al.*, 2014; *Linz et al.*, 2016]. Studies using vertical mass flux rely on reanalysis data, since this quantity is not directly observable. These studies have yet to diagnose a trend in the BDC which is reliable or robust in terms of sign or magnitude [see *Seviour et al.*, 2012; *Abalos et al.*, 2015; *Kobayashi and Iwasaki*, 2016; this study, section 3]. Thus, there is currently no clear consensus as to the observed change in the strength of the BDC.

For any climate change signal, the Time of Emergence [*Hawkins and Sutton*, 2012] is defined as the length of time after which that signal is expected to emerge from the noise of natural climate variability,

giving confidence that a significant change has been detected. In the present study, the Time of Emergence for the climate signal in the BDC trend is calculated using a long preindustrial control climate model simulation (described in section 2) to determine the length of time series that would be required to detect a 2%/decade trend in the presence of natural climate variability. The climate variability in the tropics and extratropics is removed from the trend in the BDC, using the El Niño–Southern Oscillation (ENSO) as a proxy for dynamical variability in the tropics, and the Arctic Oscillation (AO) as a proxy for dynamical variability in the extratropics (hence using DJF rather than annual means in this study), as described in section 2. While there are other measures of variability, ENSO and the AO are the main sources of interannual variability in the tropics and extratropics, respectively. Furthermore, it is well known that ENSO and the AO are related to the strength of the BDC [*Sassi et al.*, 2004; *Manzini et al.*, 2006; *García-Herrera et al.*, 2006; *Salby and Callaghan*, 2006; *Hardiman et al.*, 2007]. Results are presented in section 3, and conclusions and discussion follow in section 4.

2. Model Simulation and Definition of Indices

The model simulation analyzed in this study is a 1700 year long preindustrial control simulation, performed with all forcings fixed at 1860 levels, as described in sections 3 and 4 of *Donner et al.* [2011]. This simulation is run using the National Oceanic and Atmospheric Administration/Geophysical Fluid Dynamics Laboratory (NOAA/GFDL) global climate model CM3 [*Donner et al.*, 2011]. The GFDL CM3 model is a fully coupled atmosphere-ocean climate model. It has 48 vertical layers running from the ground to 0.01 hPa and a horizontal resolution of 200 km. It includes a fully interactive tropospheric and stratospheric chemistry scheme and explicit treatment of aerosol-cloud interaction [*Ming et al.*, 2006, 2007]. CM3 is one of the models used in support of the Intergovernmental Panel on Climate Change Fifth Assessment Report [*Intergovernmental Panel on Climate Change*, 2013].

Indices for the BDC, ENSO, and AO are used throughout this study. These indices are calculated from the data of the long control simulation as follows:

1. The monthly mean Transformed Eulerian Mean (TEM) [*Andrews et al.*, 1987; *Hardiman et al.*, 2010] vertical mass flux across 70 hPa is used to define the strength of the BDC. This mass flux is calculated by integrating the mass-weighted TEM vertical velocity, $\overline{w}^*$, across the 70 hPa pressure surface in the tropics. Here $\overline{w}^*$ is calculated by solving the TEM thermodynamic equation, as detailed in the appendix of *Lin et al.* [2015]. While it is more common to calculate $\overline{w}^*$ from the TEM momentum equation [*Andrews et al.*, 1987; *Hardiman et al.*, 2010], an accurate calculation requires 6-hourly data [see *Seviour et al.*, 2012, Figure 2]. The TEM thermodynamic equation requires only monthly data [*Lin et al.*, 2015] to produce a good approximation to $\overline{w}^*$ [see *Butchart*, 2014, section 3.2].
2. The AO index is defined as the leading Empirical Orthogonal Function of sea level pressure anomalies over the region 20°N–90°N [*Thompson and Wallace*, 1998]. The loading pattern is derived from model data.
3. The ENSO index is the Niño3.4 time series, defined as the area average of sea surface temperatures over the region 5°S–5°N and 190°E–240°E, with the time average removed [*Oliver and Irwin*, 2008].

All indices are calculated using monthly mean data and then averaged over December–January–February (DJF) for each year. In order to compare the model results with observations, use is also made of the observed AO and ENSO indices. For consistency, the observed indices are calculated using the same definitions as those for the model indices above, where

1. the observed AO index is calculated using the variance adjusted HadSLP2r data set, a near-real-time update of the HadSLP2 data set [*Allan and Ansell*, 2006]; and
2. the observed ENSO index is calculated using the HadISST data set [*Rayner et al.*, 2003].

"Observational" analyses of the BDC take the form of previous studies [*Seviour et al.*, 2012; *Abalos et al.*, 2015; *Kobayashi and Iwasaki*, 2016], which have diagnosed the BDC by using the vertical mass flux across 70 hPa in the Japanese 55 year Reanalysis (JRA55) [*Kobayashi et al.*, 2015; *Harada et al.*, 2016], ERA-Interim (ERA-I) [*Dee et al.*, 2011], and Modern Era Retrospective-Analysis for Research and Applications (MERRA) [*Rienecker et al.*, 2011] reanalysis data sets. The large spread in the vertical mass flux in reanalysis products, discussed further below, suggests that this quantity is currently more model than observation driven, especially before the start of the satellite era (1979), and the results should be viewed with this in mind.
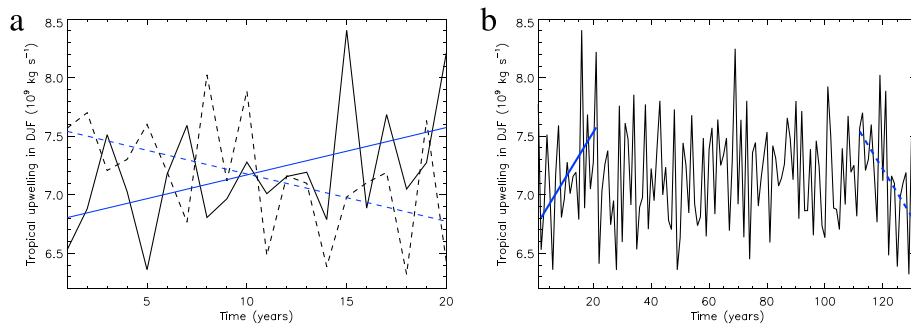
Figure 1. Example time series of the Brewer-Dobson circulation, as measured by tropical upwelling at 70 hPa in December – January – February. (a) Two 20 year periods from the long control simulation are shown, over the periods of the greatest positive (solid lines) and negative (dashed lines) trends of ±6%/decade. Model time series are shown in black, and linear regression lines are shown in blue. These trends are due to purely internal variability. (b) As in Figure 1a, but a 132 year period of the tropical upwelling time series is shown, with the blue regression lines highlighting the two 20 year periods plotted in Figure 1a.

3. Results

Using the DJF mean index for tropical upwelling (defined in the previous section) as calculated from the 1700 year long control simulation, and focusing on periods of length 10–60 years, the trend in the BDC is computed for all subsets of the data with a given period. Figure 1 shows an example of the internal variability in this trend, where for a 20 year period trends as large as ±6%/decade are found in the long control simulation. The natural variability (or uncertainty) in the BDC trend of a given period is defined as twice the standard deviation of the resulting distribution of trends for that period. Figure 2a shows that the Time of Emergence (ToE) for the expected 2% per decade climate change signal to emerge from natural variability is 28 years in the long control simulation. Using ENSO and the AO as proxies for dynamical variability in the tropics and extratropics, respectively, the uncertainty in the BDC trend due to dynamical variability can be removed by using linear regression on the 1700 year DJF mean time series of tropical upwelling against the time series for the Niño3.4 index and the AO index. Recalculating the ToE using this modified time series of tropical upwelling shows a modest reduction to 26 years, if removing either tropical or extratropical variability, or to 25 years if removing both. Using the range in the expected BDC trend (1.3–3.9% per decade) yields a range in ToE of 18–37 years, with a reduction of 1–2 years if removing either tropical or extratropical variability, and a reduction of 2–4 years if removing both. More significantly, Figure 2b shows that the uncertainty in the BDC trend is reduced
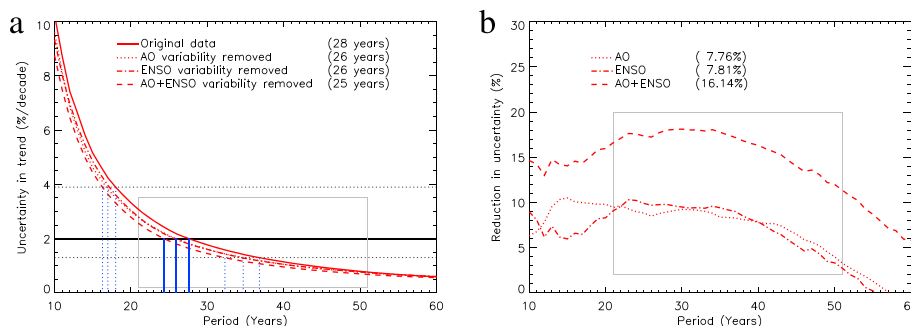

Figure 2. (a) Time of Emergence (ToE), defined as the length of time required for variability in the Brewer-Dobson circulation (BDC) trend to fall below the magnitude of the expected trend brought about by climate change. For each period, the uncertainty in the trend is defined as twice the standard deviation of the distribution of trends for that period. The trend due to climate change is defined as 2% per decade, shown as a solid black horizontal line, and the ToE is the length of period where the red curves cross this horizontal line (shown by solid vertical blue lines and also the text in brackets). The uncertainty in this trend, of 1.3–3.9% per decade, is shown by dotted black horizontal lines and the resultant range in ToE by dotted vertical blue lines. DJF seasonal means of data from the long control simulation are used in all cases. (b) Percentage reduction in trend uncertainty, due to removing the dynamical variability as diagnosed from ENSO and the AO. The average percentage reduction across periods of length 21–51 years (denoted by grey boxes) is shown, for each line, in brackets. The focus here is on periods of length 21–51 years, since this range includes all the known reanalysis-based studies, as shown in Figure 5.
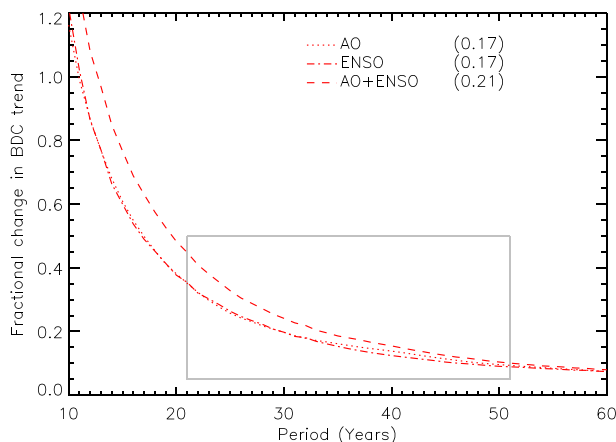
Figure 3. Proportion of BDC trend due to dynamical variability in the tropics (ENSO), extratropics (AO), and both. The change in the BDC trend is defined as a fraction of the expected 2% per decade climate signal. The average absolute fractional change across periods 21–51 years (denoted by grey box) is shown in brackets. For comparison with Figure 5, note that the fractional change due to removing AO + ENSO variability ranges from 0.45 for a 21 year period to 0.10 for a 51 year period.

by around 8% if removing either tropical or extratropical variability, and around 16% if removing both. The reduction in uncertainty becomes large at very short periods (not shown), is relatively constant over periods of length 10–40 years, and becomes negligible for periods longer than 60 years.

The difference between the trends in the modified time series of tropical upwelling (i.e., with the influence of the AO and ENSO removed) and the trends in the original upwelling time series, gives a measure of the absolute change in the trend of the BDC which is due to dynamical variability (Figure 3). As in Figure 2b,
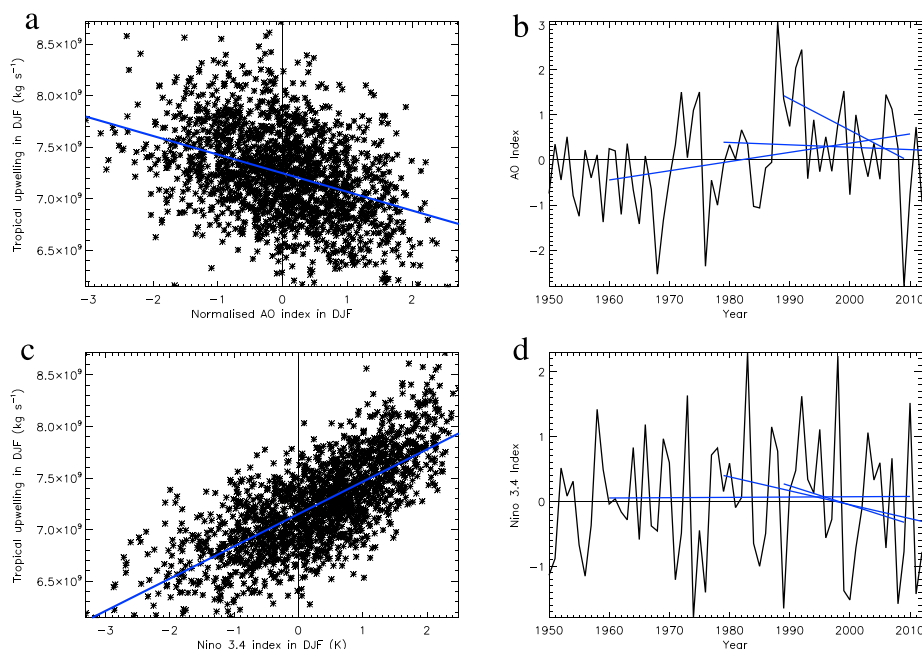
Figure 4. DJF seasonal means of tropical upwelling scatterplotted against DJF seasonal means of (a) the normalized AO index and (c) the Niño 3.4 index from the 1700 year long control simulation (thus, each plot contains 1699 asterisks). For simple linear regression, interannual regression coefficients between tropical upwelling and the AO/Niño 3.4 indices are the gradients of the blue lines. For comparison with existing studies (see Figure 5), the observed trends in (b) the AO and (d) ENSO are calculated over the periods 1989–2009, 1979–2012, and 1960–2010, again using DJF seasonal mean data. AO and ENSO indices are shown as black lines. The values of the trends (shown as blue lines) are 1989–2009: $-6.97\text{e}-2\ \text{yr}^{-1}$ (AO) and $-2.96\text{e}-2\ \text{K/yr}$ (ENSO); 1979–2012: $-5.27\text{e}-3\ \text{yr}^{-1}$ (AO) and $-2.14\text{e}-2\ \text{K/yr}$ (ENSO); and 1960–2010: $2.04\text{e}-2\ \text{yr}^{-1}$ (AO) and $4.68\text{e}-4\ \text{K/yr}$ (ENSO).
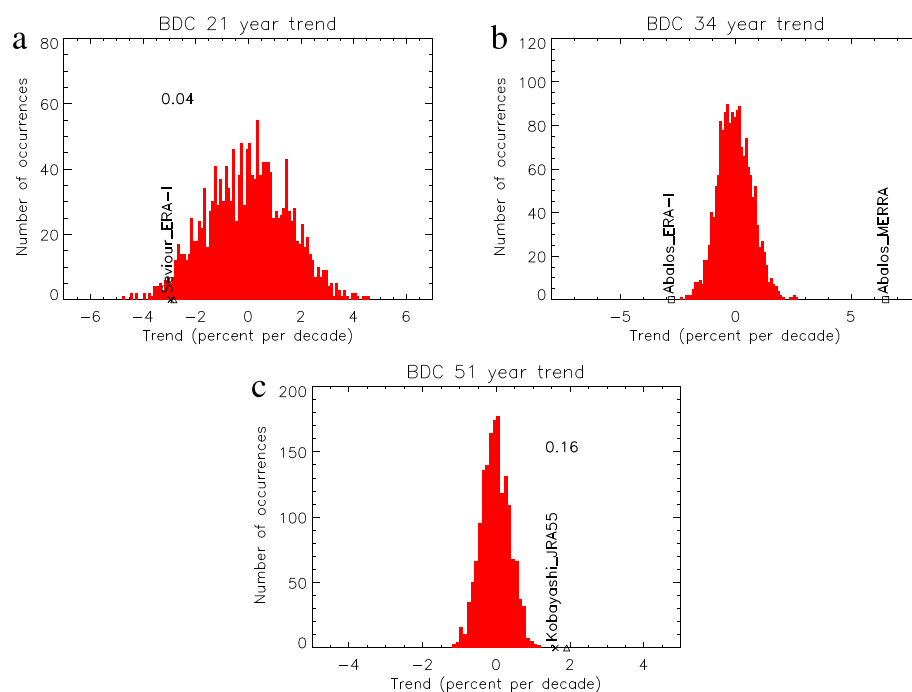
Figure 5. Shown are the BDC trends for (a) Seviour et al. (for period 1989–2009 using ERA-I), (b) Abalos et al. (for period 1979–2012 using ERA-I and MERRA), and (c) Kobayashi et al. (for period 1960–2010 using JRA55). Raw trends (all using DJF means) are marked by crosses. The trends given in Abalos et al. have already been corrected for dynamical variability due to ENSO (and the QBO) and are marked by squares. BDC trends that have been corrected for climate variability in the present study (i.e., trends with the dynamical variability as diagnosed from the AO and ENSO removed) are marked by triangles. The fractional change (cf. Figure 3) in the corrected trend, due to the influence of dynamical variability being removed, is shown above the cross marks in each panel. The histograms show the variability in BDC trends as calculated from the long control simulation for periods of 21 years (Figure 5a), 34 years (Figure 5b), and 51 years (Figure 5c).

the individual impacts of the AO and ENSO on the BDC trend are found to be very similar. This feature is potentially model dependent and is somewhat surprising given that the model AO index exhibits greater variability than the ENSO index for most periods longer than 7 years (not shown). For relatively short periods (< ~12 years) the dynamical variability represented by the AO and ENSO can completely cancel out the trend in the BDC (i.e., the fractional change shown in Figure 3 is ≥1.0 for such short periods).

These conclusions—both the ToE of around 30 years for a 2% per decade BDC trend (with a range in ToE of around 20–40 years for a range of 1.3–3.9% per decade in BDC trend) and the potential cancelation of the BDC trend by dynamical variability for periods less than around 12 years—are not model dependent, as demonstrated in the supporting information to this manuscript.

We now assess whether the results above, diagnosed using the long control simulation, are likely to be relevant to estimates of the BDC trend as calculated from reanalysis data in existing studies. This requires the regression coefficients (between the BDC and the AO and ENSO), taken here from the long control simulation (Figures 4a and 4c), and the trends in the *observed* AO and ENSO indices over the periods corresponding to existing studies (Figures 4b and 4d). For removal of the combined influence, the multiple linear regression coefficients for the AO [−1.12e+8 (kg/s)] and ENSO [2.91e+8 (kg/s/K)] with the tropical upwelling, and the trends in Figures 4b and 4d, need to be used along with the observed average tropical upwelling in DJF [calculated as 7.1e+9 (kg/s) using ERA-I data].

Figure 5 shows the BDC trend as calculated from reanalysis data in three previous studies (for the periods 1989–2009, 1979–2012, and 1960–2010), along with "corrected" trends with the influence of dynamical variability removed (for all except 1979–2012, where ENSO variability is removed in the original study). The vertical velocities in reanalysis data sets are in general very noisy [see *Butchart*, 2014, section 5.1], as demonstrated by the huge spread in observed trends across the different reanalyses (already noted by *Abalos et al.* [2015]), ranging from −2.9%/decade to +6.5%/decade (marked by cross symbols for raw trends and squares

and triangles for corrected trends as shown in Figure 5). Indeed, the trend is negative in the ERA-I reanalysis, whereas a positive trend is expected due to climate change (and found in the MERRA and JRA55 reanalyses). *Abalos et al.* [2015] also found that the trend in JRA55 over the satellite era (i.e., the 34 year period used here) is not statistically significant. Clearly, then, better observational analyses of tropical upwelling are still required. As demonstrated by Figures 2 and 3 above, around 30 years of such data would be necessary for the climate signal in the BDC trend to emerge, and for data sets $<\sim$12 years in length, dynamical variability again has the potential to completely mask any trend in the BDC.

Figure 3 further predicts that removing dynamical variability will give rise to a mean fractional change in the BDC trend of 0.45 for a 21 year period and 0.10 for a 51 year period. The 95% confidence intervals for these fractional changes are [0,1.12] and [0,0.25], respectively (assuming a half-normal distribution, since we compute the absolute fractional change). The observed fractional changes, diagnosed from the reanalyses, are calculated to be 0.05 for a 21 year period and 0.15 for a 51 year period, when defined as a fraction of a 2%/decade trend to allow direct comparison with Figure 3 (these changes are also shown in Figure 5b, calculated as fractions of the observed corrected trends). Despite the large uncertainty across different reanalyses, these observed values agree well with those predicted, and both observed corrections lie within the calculated 95% confidence intervals from the model.

In addition, the histograms in Figure 5 show the variability in the BDC trends as calculated from the long control simulation and give an indication as to whether or not the observed trends fall within or outside of natural variability during these periods. In good agreement with the $\sim$30 year ToE calculated in Figure 2, the 21 year trend falls within natural variability, the 34 year trend is on the edge of natural variability (dependent on the reanalysis data set used), and only the 51 year trend is outside of the expected natural variability.

4. Conclusions

The trend in the Brewer-Dobson circulation (BDC), its Time of Emergence (ToE), and the fractional change in trend due to removing the impacts of dynamical variability are investigated using a long preindustrial control simulation. The ToE of the expected 2% per decade trend in the BDC is 28 years in the long control simulation. There is a modest reduction of this time to 26 years if removing dynamical variability in the tropics (as represented by the El Niño–Southern Oscillation, ENSO) or the extratropics (as represented by the Arctic Oscillation, AO). There is a reduction of the ToE to 25 years if removing variability in both regions. Assuming an uncertainty in the expected BDC trend of 1.3–3.9% per decade [*Butchart et al.*, 2010; *Butchart*, 2014] yields a ToE in the range 18–37 years, with a modest reduction in this ToE of 2–4 years if removing variability in both the tropics and extratropics. Furthermore, for periods of 21–51 years in length, dynamical variability accounts for around 20% of the uncertainty in the BDC trend.

The predictions made using the long control simulation have been compared with real-world data, using the BDC trends calculated from reanalysis data in three existing studies and correcting these trends by removing the effects of dynamical variability. Although there is a huge spread in vertical velocity across different reanalysis data sets, making the observed change in the BDC very difficult to determine, the reanalyses are in broad agreement with the conclusions drawn from model data in the following regard:

1. The simulated fractional change in the BDC trend due to dynamical variability lies within the intervals [0,1.12] for a 21 year period and [0,0.25] for a 51 year period, with 95% confidence. The observed corrections, calculated as fractions of a 2%/decade trend, are 0.05 for a 21 year period and 0.15 for a 51 year period and lie within the simulated 95% confidence intervals.
2. The calculated ToE of $\sim$30 years for the 2%/decade BDC trend is consistent with observed trends in the BDC falling within expected natural variability for a 21 year period, close to the edge of expected variability for a 34 year period and outside of expected variability for a 51 year period.

For shorter periods, the impact of dynamical variability on the BDC trend is much greater, having the potential to completely cancel out the observed trend in the BDC for periods less than $\sim$12 years. Given the huge variability in the observed BDC trend across current reanalysis data sets, this suggests that better observational analyses of tropical upwelling will be required for an extended period before any firm conclusions can be drawn with regard the impact of climate change on the BDC.

References

Abalos, M., B. Legras, F. Ploeger, and W. J. Randel (2015), Evaluating the advective Brewer-Dobson circulation in three reanalyses for the period 1979–2012, *J. Geophys. Res. Atmos.*, *120*, 7534–7554, doi:10.1002/2015JD023182.

Allan, R., and T. Ansell (2006), A new globally complete monthly historical gridded mean sea level pressure dataset (HadSLP2): 1850–2004, *J. Clim.*, *19*, 5816–5842, doi:10.1175/JCLI3937.1.

Andrews, D. G., J. R. Holton, and C. B. Leovy (1987), *Middle Atmosphere Dynamics, International Geophysical Series*, vol. 40, 489 pp., Academic Press, San Diego, Calif.

Birner, T., and H. Boenisch (2011), Residual circulation trajectories and transit times into the extratropical lowermost stratosphere, *Atmos. Chem. Phys.*, *11*, 817–827, doi:10.5194/acp-11-817-2011.

Butchart, N., and A. A. Scaife (2001), Removal of chlorofluorocarbons by increased mass exchange between the stratosphere and troposphere in a changing climate, *Nature*, *410*, 799–802, doi:10.1038/35071047.

Butchart, N., et al. (2006), Simulations of anthropogenic change in the strength of the Brewer-Dobson circulation, *Clim. Dyn.*, *27*, 727–741, doi:10.1007/s00382-006-0162-4.

Butchart, N., et al. (2010), Chemistry-climate model simulations of 21st century stratospheric climate and circulation changes, *J. Clim.*, *23*, 5349–5374, doi:10.1175/2010JCLI3404.1.

Butchart, N. (2014), The Brewer-Dobson circulation, *Rev. Geophys.*, *52*, 157–184, doi:10.1002/2013RG000448.

Dee, D. P., et al. (2011), The ERA-Interim reanalysis: Configuration and performance of the data assimilation system, *Q. J. R. Meteorol. Soc*, *137*, 553–597, doi:10.1002/qj.828.

Donner, L. J., et al. (2011), The dynamical core, physical parameterizations, and basic simulation characteristics of the atmospheric component AM3 of the GFDL global coupled model CM3, *J. Clim.*, *24*, 3484–3519, doi:10.1175/2011JCLI3955.1.

Engel, A., et al. (2009), Age of stratospheric air unchanged within uncertainties over the past 30 years, *Nat. Geosci.*, *2*, 28–31, doi:10.1038/ngeo388.

Fu, Q., P. Lin, S. Solomon, and D. L. Hartmann (2015), Observational evidence of strengthening of the Brewer-Dobson circulation since 1980, *J. Geophys. Res. Atmos.*, *120*, 10,214–10,228, doi:10.1002/2015JD023657.

García-Herrera, R., N. Calvo, R. R. Garcia, and M. A. Giorgetta (2006), Propagation of ENSO temperature signals into the middle atmosphere: A comparison of two general circulation models and ERA-40 reanalysis data, *J. Geophys. Res.*, *111*, D06101, doi:10.1029/2005JD006061.

Garny, H., T. Birner, H. Bönisch, and F. Bunzel (2014), The effects of mixing on age of air, *J. Geophys. Res. Atmos.*, *119*, 7015–7034, doi:10.1002/2013JD021417.

Harada, Y., H. Kamahori, C. Kobayashi, H. Endo, S. Kobayashi, Y. Ota, H. Onoda, K. Onogi, K. Miyaoka, and K. Takahashi (2016), The JRA-55 reanalysis: Representation of atmospheric circulation and climate variability, *J. Meteorol. Soc. Jpn.*, *94*, 269–302, doi:10.2151/jmsj.2016-015.

Hardiman, S. C., N. Butchart, P. H. Haynes, and S. H. E. Hare (2007), A note on forced versus internal variability of the stratosphere, *Geophys. Res. Lett.*, *34*, L12803, doi:10.1029/2007GL029726.

Hardiman, S. C., D. G. Andrews, A. A. White, N. Butchart, and I. Edmond (2010), Using different formulations of the transformed Eulerian mean equations and Eliassen-Palm diagnostics in general circulation models, *J. Atmos. Sci.*, *67*, 1983–1995, doi:10.1175/2010JAS3355.1.

Hardiman, S. C., N. Butchart, and N. Calvo (2014), The morphology of the Brewer-Dobson circulation and its response to climate change in CMIP5 simulations, *Q. J. R. Meteorol. Soc.*, *140*, 1958–1965, doi:10.1002/qj.2258.

Hawkins, E., and R. Sutton (2012), Time of emergence of climate signals, *Geophys. Res. Lett.*, *39*, L01702, doi:10.1029/2011GL050087.

Intergovernmental Panel on Climate Change (2013), *Climate Change 2013: The Physical Science Basis. Contribution of Working Group I to the Fifth Assessment Report of the Intergovernmental Panel on Climate Change*, edited by T. F. Stocker et al., 1535 pp., Cambridge Univ. Press, Cambridge, U. K., and New York.

Kobayashi, C., and T. Iwasaki (2016), Brewer-Dobson circulation diagnosed from JRA-55, *J. Geophys. Res. Atmos.*, *121*, 1493–1510, doi:10.1002/2015JD023476.

Kobayashi, S., et al. (2015), The JRA-55 reanalysis: General specifications and basic characteristics, *J. Meteorol. Soc. Jpn.*, *93*, 5–48, doi:10.2151/jmsj.2015-001.

Lin, P., and Q. Fu (2013), Changes in various branches of the Brewer-Dobson circulation from an ensemble of chemistry climate models, *J. Geophys. Res. Atmos.*, *118*, 73–84, doi:10.1029/2012JD018813.

Lin, P., Y. Ming, and V. Ramaswamy (2015), Tropical climate change control of the lower stratospheric circulation, *Geophys. Res. Lett.*, *42*, 941–948, doi:10.1002/2014GL062823.

Linz, M., R. Plumb, E. Gerber, and A. Sheshadri (2016), The relationship between age of air and the diabatic circulation of the stratosphere, *J. Atmos. Sci.*, *73*, 4507–4518, doi:10.1175/JAS-D-16-0125.1.

Manzini, E., M. A. Giorgetta, M. Esch, L. Kornblueh, and E. Roeckner (2006), The influence of sea surface temperatures on the northern winter stratosphere: Ensemble simulations with the MAECHAM5 model, *J. Clim.*, *19*, 3863–3881.

Ming, Y., V. Ramaswamy, L. J. Donner, and V. T. J. Phillips (2006), A new parameterization of cloud droplet activation applicable to general circulation models, *J. Atmos. Sci.*, *63*, 1348–1356, doi:10.1175/JAS3686.1.

Ming, Y., V. Ramaswamy, L. J. Donner, V. T. J. Phillips, S. A. Klein, P. Ginoux, and L. W. Horowitz (2007), Modeling the interaction between aerosols and liquid water clouds with a self-consistent cloud scheme in a general circulation model, *J. Atmos. Sci.*, *64*, 1189–1209, doi:10.1175/JAS3874.1.

Moss, R. H., et al. (2010), The next generation of scenarios for climate change research and assessment, *Nature*, *463*, 747–756, doi:10.1038/nature08823.

Nakicenovic, N., and R. Swart (Eds.) (2000), *Special Report on Emissions Scenarios*, 570 pp., Cambridge Univ. Press, Cambridge, U. K.

Oliver, M. J., and A. J. Irwin (2008), Objective global ocean biogeographic provinces, *Geophys. Res. Lett.*, *35*, L15601, doi:10.1029/2008GL034238.

Rayner, N. A., D. E. Parker, E. B. Horton, C. K. Folland, L. V. Alexander, D. P. Rowell, E. C. Kent, and A. Kaplan (2003), Global analyses of sea surface temperature, sea ice, and night marine air temperature since the late nineteenth century, *J. Geophys. Res.*, *108*(D14), 4407, doi:10.1029/2002JD002670.

Riahi, K., A. Gruebler, and N. Nakicenovic (2007), Scenarios of long-term socio-economic and environmental development under climate stabilization, *Technol. Forecasting Social Change*, *74*, 887–935.

Rienecker, M. M., et al. (2011), MERRA: NASA's Modern-Era Retrospective Analysis for Research and Applications, *J. Clim.*, *24*, 3624–3648, doi:10.1175/JCLI-D-11-00015.1.

Salby, M. L., and P. F. Callaghan (2006), Influence of the Brewer-Dobson circulation on stratosphere-troposphere exchange, *J. Geophys. Res.*, *111*, D21106, doi:10.1029/2006JD007051.

Sassi, F., D. Kinnison, B. A. Boville, R. R. Garcia, and R. Roble (2004), Effect of El Niño–Southern Oscillation on the dynamical, thermal, and chemical structure of the middle atmosphere, *J. Geophys. Res.*, *109*, D17108, doi:10.1029/2003JD004434.

Seviour, W. J. M., N. Butchart, and S. C. Hardiman (2012), The Brewer-Dobson circulation inferred from ERA-Interim, *Q. J. R. Meteorol. Soc.*, *138*, 878–888, doi:10.1002/qj.966.

Thompson, D. W. J., and J. M. Wallace (1998), The Arctic oscillation signature in the wintertime geopotential height and temperature fields, *Geophys. Res. Lett.*, *25*(9), 1297–1300, doi:10.1029/98GL00950.

Walters, D., et al. (2017), The Met Office unified Model Global Atmosphere 6.0/6.1 and JULES Global Land 6.0/6.1 configurations, *Geosci. Model Dev. Discuss.*, doi:10.5194/gmd-2016-194, in review.

Waugh, D. W. (2009), Atmospheric dynamics: The age of stratospheric air, *Nat. Geosci.*, *2*, 14–16, doi:10.1038/ngeo397.

Williams, K. D., et al. (2015), The Met Office Global Coupled model 2.0 (GC2) configuration, *Geosci. Model Dev.*, *8*, 1509–1524, doi:10.5194/gmd-8-1509-2015.